Miniaturised SH EMATs for fast robotic screening of wall thinning in steel plates

O Trushkevych, M Tabatabaeipour, S Dixon, MDG Potter, G Dobie, C MacLeod and RS Edwards

***Abstract*— Electromagnetic acoustic transducers (EMATs) are well suited to generating and detecting a variety of different ultrasonic wavemodes, without the need for couplant, and they can be operated through some coatings. EMATs can be used to generate shear horizontal (SH) waves, which show promise for fast screening of wall thinning and other defects. However, commercial SH-wave EMATs are not suitable for robotic implementation on ferritic steel due to the large magnetic drag force from the magnets. This paper describes the design and characterisation of miniaturised SH guided wave EMATs, which significantly reduce the magnetic drag and enable mounting onto a small crawler robot for sample scanning. The performance of the miniaturised EMATs is characterised and compared to a commercial EMAT. It is shown that signal to noise ratio is reduced, but remains within an acceptable range to use on steel. The bandwidth and directivity are increased, depending on the exact design used. Their ability to detect flat bottomed holes mimicking wall thinning is also tested.**

***Index Terms*— Condition monitoring, electromagnetic devices, non-destructive testing, ultrasonic transducers.**

I. Introduction

THERE is a growing need for faster, more reliable, automated inspection of a variety of structures and materials. Robotic inspection is a potential solution for automated inspection; however, current inspection techniques use point-by-point scanning, accumulating large amounts of data and requiring operator presence and input [1]. Point-by-point scanning typically uses ultrasound (longitudinal or shear wavemodes at normal incidence to sample surface) to measure the thickness of the material at each point and detect defects. This is normally done using a piezoelectric transducer, which requires couplant and consistent contact with the material under test. Non-contact methods of inspection are preferable as they can simplify the process [2].

Significantly faster screening for defects in plates could be achieved by using guided waves, such as Lamb or shear horizontal (SH) waves [3], instead of point-by-point measurements. Guided SH waves are complicated to generate using piezoelectric transducers, but can be generated easily by electromagnetic acoustic transducers (EMATs). These are non-contact ultrasonic transducers, which can generate a variety of wavemodes in conducting samples without direct contact with the sample, and can be operated through some coatings [4] [5] [6] [7] [8] [9] [10] [11].

EMATs used for commercial thickness gauging on plate structures analyse reflections of bulk waves, and typically consist of a large single magnet plus a coil of wire [12]. For generation of SH waves, the periodic permanent magnet (PPM) configuration described below is the standard commercially used EMAT design, and these contain a large number of smaller magnets [4] [5]. Both designs experience a large magnetic drag when inspecting magnetic samples such as ferritic steel, and this means that automated scanning using crawler robots on magnetic samples is not currently feasible. One solution for robotic inspection using EMATs would be to use an electromagnet in place of the permanent magnet [13]. This has been investigated previously for controlling the type of waves generated, and would contribute to the ease of movement of the robot, with the electromagnet switched off during motion and on during inspection, but would add extra weight, cabling and complexity.

We have recently produced miniaturised EMATs containing permanent magnets, generating and detecting Rayleigh waves for characterisation of surface-breaking defects on metals [14]. The miniaturisation had the benefits of reducing magnetic drag and overall weight, thus simplifying the inspection process, and in addition improving spatial resolution. This paper presents new miniaturised EMAT designs for generating and detecting SH guided waves, and demonstrates their use for automated scanning using robotic crawlers, considering the suitability of the generated ultrasound waves, and the magnetic drag for different designs. The target inspection challenge is wall thinning in mild steel plates, for structures such as storage tanks; a 10 mm thick steel plate is used as a sample. The magnetic drag and signal to noise ratio (SNR) are compared with standard commercial SH wave EMATs. Miniaturised EMATs are tested on a sample containing an artificial defect, showing an example of how they could be applied during testing.

The work has been done on the RCNDE Core Research Programme 2018-20, Remote and Automated Delivery of Non-Contact NDE Sensors. RCNDE is funded by industry and by EPSRC grant no. EP/L022125/1.

OT, SD and RSE are at Department of Physics, University of Warwick, Coventry, UK. MT, CM and GD are at School of Engineering, University of Strathclyde, Glasgow, UK. MDGP is at Sonemat Ltd., Coventry, UK. Email: r.s.edwards@warwick.ac.uk, o.trushkevych@warwich.ac.uk

II. Guided SH waves and EMAT design

EMATs for generating and detecting SH waves are typically produced using a racetrack coil design and a set of magnets in a PPM configuration [10] [11]. This gives a wavelength determined by the size and spacing of the magnets [5]. The choice of wavelength and frequency of operation is made through analysing phase speed dispersion curves for different modes. The phase (c_p) and group (c_g) velocity dispersion curves for homeotropic homogeneous materials are calculated using the following equations [3],

$$c_p = \pm 2c_s \frac{fd}{\sqrt{4(fd)^2 - n^2 c_s^2}}, \quad (1)$$

$$c_g = c_s \sqrt{1 - \left(\frac{nc_s}{2fd}\right)^2}, \quad (2)$$

where c_s is bulk shear wave velocity, d is plate thickness, f is frequency and n is the mode number. Note that for $n = 0$, corresponding to the SH_0 mode, $c_p = c_g = c_s$.

Figure 1 shows the dispersion curves for the first four SH modes, together with lines of equal wavelength for three different wavelengths, calculated for the steel plate inspected in this work. Experimental measurement of the SH_0 speed in the chosen plate was used to obtain c_s and hence calculate the dispersion curves for the specific sample under study. Signals will be generated where the line for the wavelength set by the magnet spacing crosses the dispersion curve for each wavemode, and this governs the choice of excitation frequency for the chosen plate thickness and mode [5].

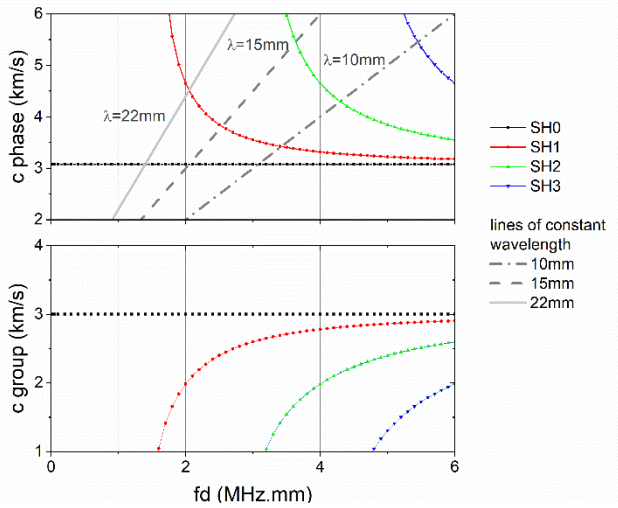

Figure 1: Dispersion curves for SH waves, produced for 10 mm thick steel plate, for (a) phase and (b) group velocity. Lines of constant wavelength are added to the phase velocity curves to illustrate wavelength and frequency/wavemode selection.

A variation in the plate thickness d will change the frequency-thickness product $f.d$. The group velocities of the dispersive modes, and their gradients, will therefore change when the plate thickness changes. In addition, modes that can no longer be supported in the thinner regions (below the cut-off frequency-thickness) will mode convert or reflect, and their amplitude will be affected [6] [7]. Gradual wall thinning in plates has been successfully detected using the SH_1 wavemode in the region of high dispersion (steep gradient), using reflection and transmission measurements [6] [7]. Wall thinning has been identified through measuring the cut-off frequency for higher order SH modes, with this sensitive to the maximal extent of the wall thinning [15]. Mode conversions and reflections depend on the tapering angle of the wall thinning, and therefore SH wave inspection is not suitable for detailed defect characterisation [15]. However, it is promising for fast screening and highlighting defective regions, and then other types of inspection, such as point thickness measurements, can be employed to characterise defects in more detail, if desired. For screening, inspection using a combination of cut-off frequency, changes in arrival time, mode conversions, and transmitted or reflected wave amplitudes has been suggested [15].

Generation of just the SH_0, or the SH_0 and SH_1 modes, can be beneficial for data analysis, with a dispersive SH_1 mode having advantages in thickness gauging. This study aims to generate the SH_1 wavemode in the region of high dispersion on 10 mm thick steel. A nominal wavelength of 22 mm was chosen, because its line of constant wavelength crosses the SH_1 mode on the dispersion curve at a region of higher dispersion compared to the lines for 10 mm or 15 mm wavelengths (Figure 1a). For a 10 mm thick steel sample, excitation around 200 kHz was used for efficient generation of SH_1.

A. EMAT design considerations

The standard racetrack coil and PPM EMAT design is shown in Figure 2, left hand design. The PPM array periodicity sets the wavelength, as shown in the figure. A periodic force structure which generates an SH wave can be obtained through the Lorentz force or magnetostriction. Magnetostrictive effects can be significant on magnetite [16] [17], but are negligible in the tested samples. The Lorentz force is the force on particles of charge q moving with velocity $\boldsymbol{v}$ in a magnetic field $\boldsymbol{B}$, given by $\boldsymbol{F}=q\boldsymbol{v}\times\boldsymbol{B}$. Some variations on coil and magnet design have been suggested previously. These are based around the same principle of operation, having the same periodicity for the force profile. For example, Choi et al. use triple racetrack coils and a 6x6 magnet array rather than a single coil and 2x6 magnet array [18]. This force profile generates a narrowband, directional signal. Ribichini et al. use a linear coil wrapped around an array of magnets [16]. Focusable SH wave EMATs have been developed using cooperation of two rotatable transducers [19], or a fan-shaped PPM array with an oblique angle [20]. All of these designs require a large number of magnets.

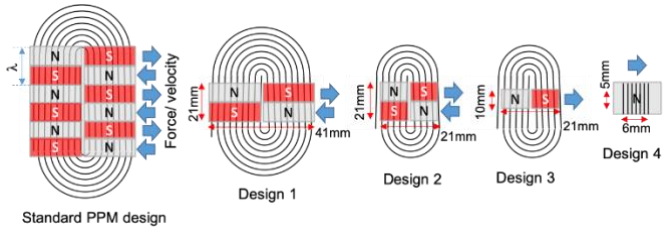

Figure 2: Standard and miniature SH EMAT designs. Small arrows and numbers show active area in mm. Magnet polarisation direction is shown by letters N and S. Large arrows indicate the direction of force (generation) / wave velocity (detection). The size of the active area of a commercial EMAT with 20 mm wavelength used in this study is 40 x 60 mm. Designs 1 & 2 generate at 22 mm wavelength according to magnet periodicity. Wavelength is less strictly defined for designs 3 and 4.

The large permanent magnets and arrays of magnets used in these designs create difficulties when scanning on ferritic

samples, as magnetic attraction to the sample can significantly complicate scanning. When trying to move EMATs on ferritic steel plates using robots, there is a tight limit on the load that the robot can push or pull [21]. The drag/push forces experienced by the robot will depend on the combination of magnetic forces, EMAT weight, and friction. The simplest way to reduce the drag force is by reducing friction – for example using rolling friction instead of drag friction, by putting EMATs into cases which are attached to rollers. The overall coefficient of friction k_{fr} depends on the roller radius r,

$$k_{fr}=k_l/r, \quad (3)$$

where k_l is the rolling friction coefficient. Note that "rolling friction coefficient" is often used in the literature to identify the dimensionless value k_{fr}, which depends on the roller radius and k_l [m], which is a parameter dependent only on the materials interacting.

A further step to ease scanning is to decrease magnetic attraction to the sample. Previously this has been done for scanning EMAT inspection using different wavemodes by increasing the lift-off of the magnet while keeping the coil close to the sample, or using just the dynamic magnetic field from the current pulse through the coil for generation [22]. These approaches, however, cannot be adapted to generate SH waves. Another option which can be used with the PPM SH wave EMAT design is to increase lift-off of the whole EMAT; this reduces magnetic attraction, making scanning easier, but also decreases SNR.

The novelty of the current work is in challenging the notion that only highly periodic systems can be used for SH wave generation. We change the design of the EMATs to reduce the number of magnets used and hence reduce magnetic drag, with the new designs shown in Figure 2. Design 1 reduces the number of magnets so that only two opposing forces are generated, but keeps the coil and magnet widths the same to produce a wavefront of the same width as the standard design. This would have the least effect on EMAT directional properties compared to the design with multiple magnets. The wavelength is still set by the length of the magnets. EMAT size can be further reduced by using the smaller wavefront (narrower magnets) design shown in Design 2, which also uses a narrower coil. Taking miniaturisation further, an EMAT with a racetrack coil and an array of only two magnets, with a single force for generation, was made and is labelled as Design 3. The ultimate miniaturisation was achieved by making an EMAT which was a linear coil wound around a single magnet – Design 4, where the coil length is in the direction of wave propagation, which is primarily designed for detection. Coils were hand-wound using wire of diameter 0.35 mm for designs 1 and 2, 0.2 mm for design 3 and 0.14 mm for design 4.

The miniaturisation process results in reduced magnetic attraction: the SNR is inevitably decreased, however, the decrease is less pronounced compared to the change with increasing EMAT lifotff, and the new designs offer a significant reduction in magnetic drag with minimised reduction in SNR. The EMATs will also be more broadband, as fewer restrictions are put on enforcing a particular wavelength. The latter is not necessarily a drawback as the required bandwidth depends on the desired application, and a larger bandwidth can be beneficial in methods that rely on analysing several wavemodes [6] [15] [23]. Reducing the width of the wavefront (designs 2-4) allowed the use of smaller coils with fewer turns, which are expected to have a shorter "dead time" – the time during which the receiving electronics is saturated – thus allowing the generator and detector to be brought closer together, similar to the EMATs reported in [14]. The dead time depends on factors including the sample, transducer impedance, and external shielding, and reducing the coil size reduces the impedance. This may be required in some applications, in particular on small or narrow samples. The expected trade-off for using EMATs with a width of the wavelength or smaller is reduced directivity of the EMAT [17]. This may not be significant in applications where travel distance of the signals of interest is under 40 cm, but may not be acceptable where signals need to travel longer distances.

In standard SH wave measurements, identical pairs of PPM-EMATs are used: one for generation and one for detection [7] [15] [18]. Alternatively, the same EMAT can be used for generation and detection, but this set-up suffers from electrical noise and a longer dead time [5]. Both of these set-ups ensure that the measurements are narrowband and therefore have a reduced sensitivity to mode-converted wavemodes. This paper explores the possibility of using unmatched pairs, where detectors are smaller than generators, in order to reduce the magnetic drag as much as possible.

All miniature EMATs can be used as generators or detectors, with designs 1 - 3 better suited for generation, and all designs suitable for detection. EMATs with designs 3 and 4, when used as detectors, detect the SH wavemodes generated, and may also detect mode converted signals. This may be useful in scenarios where sensitivity to a variety of wavemodes is required, such as when using mode conversions as indicative of a defect [6] [15] [24] [23]. Size miniaturisation of detectors can also offer the extra benefit of providing higher spatial resolution when scanning, in particular in the near field, and higher sensitivity to defects with small lateral dimensions [14] [25].

III. Methodology

The new designs of EMATs were evaluated by testing which modes they generate and detect, their directivity, SNR, and magnetic drag forces on a ferritic steel sample when mounted on a small crawler robot. A commercial EMAT pair (produced by Sonemat Ltd) was used for comparison. Defect detection capabilities of miniature EMATs were then evaluated. The miniaturised EMATs were designed to have a wavelength of 22 mm.

Two steel plates with 10 mm thickness were used as samples. The first had dimensions of 1500×1500 mm, and the second had dimensions of 300×1500 mm. The larger plate was used for EMAT characterisation (directivity, SNR, SH_0 speed) to minimise the effect of edge reflections. The smaller plate had several flat bottomed holes which were used as calibration defects. Generation and detection EMATs were set up in a pitch-catch arrangement, as shown in Figure 3 (a). The separation between EMATs was set as 300 mm for most measurements. This separation was chosen to give a balance between minimising the effects of dead-time, limiting edge reflections, and offering suitable resolution for defects. When scanning over a defect the whole area between the transducers will be flagged up as potentially defective while the defect is

between the EMATs. Multiple scans in different directions over the same area will be necessary to narrow this area down further.

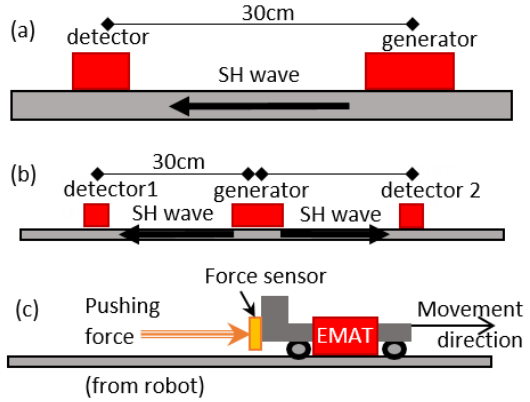

Figure 3: Setups used in the study: (a) pitch-catch arrangement for wall thinning monitoring; (b) suggested double pitch-catch arrangement to cover larger areas in a single scan; (c) setup for measuring pushing force to move EMAT on steel.

A low frequency RITEC Pulser/ Receiver RPR4000-0.05-1 was used to drive the generation EMATs, using either 1, 3 or 6 cycles, with 3 cycle excitation shown to be optimal for further studies. Directivity of the miniature EMATs was tested by keeping the detection EMAT in a fixed position. The generator was also held in the same position with the help of a guide, and rotated. In this way irregularities in the sample or lift-off variations of the detector were avoided. The detector with the smallest active area was used for directivity testing (Design 4), and the distance between the generator and detector was set to 500 mm to maximise angular resolution.

The SH_0 speed was measured on the larger plate. A single measurement of arrival time of a mode contains uncertainty in the triggering delay. To measure the SH_0 speed with better precision, the transducers were excited at 100 kHz to generate the SH_0 mode only and placed at different separation distances, from 30 cm to 60 cm with 5 cm step size. A linear fit of the arrival times of the SH_0 mode as a function of separation distance was used to find the speed of SH_0, 3075 ± 6 m/s.

SH wave generation is bi-directional when using PPM EMAT designs. This can complicate inspection, and focusing using two generation EMATs [13] or interlacing wedge-shaped segments of PPM and coils of different phases [26] has previously been suggested as a method to suppress the unwanted direction. However, this phenomenon can be an advantage in high speed inspection. If two detectors are placed with one on either side of the generator, a larger area can be covered in one scan (Figure 3(b)). Using two detectors can also help separate echoes coming from different sides of the sample [27].

The EMATs were mounted in cases with rollers, and an Inktun miniature magnetic crawler (Inuktun VT100 MicroMag Crawler System) was used to push the EMATs on an uncorroded steel plate to test the magnetic drag and the ability to scan using the EMATs. The manufacturer specification of the pulling/pushing capacity for the robot is: normal pull 5.5 kg; short term pull 9 kg; peak pull 13.5 kg [21]. The force experienced by the robot pushing a wheeled holder containing an EMAT was measured for each individual transducer using a SingleTact force sensor [28]. The arrangement for the force measurement is shown in Figure 3(c). A roller with radius r = 2.5mm was used for the miniature EMATs. A larger roller with r = 7.5 mm was used for the commercial EMATs to further reduce drag force, as otherwise they could not be moved. The estimated difference in friction coefficient for the commercial EMATs was proportional to the difference in roller radius, hence the drag force was reduced by a factor of three compared to the smaller roller. The drawback of using a larger roller is lower precision in defining lift-off of the EMAT, and larger lift-off variations. Note that where the sample is corroded or not smooth, the friction (and the drag force) will increase.

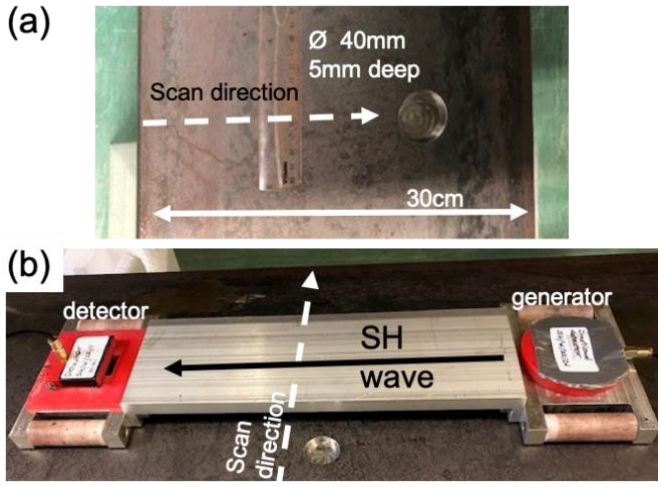

Figure 4: (a) sample with defect; (b) photograph of the scan arrangement in pitch-catch geometry.

To evaluate defect detection capabilities, an EMAT pair was scanned on a 10 mm thick steel sample containing a 5 mm deep, 40 mm diameter flat bottomed hole (Figure 4(a)). The transducers were arranged in a pitch-catch geometry as shown in Figure 4(b). The defect was kept in the middle between the generator and detector as this was found to be the worst case scenario for detection. Manual scanning was used for these tests. It was not possible to scan the commercial pair over the defect manually due to the magnetic drag.

IV. Experimental Results

A. Mode generation

When exciting the EMATs at 200 kHz (frequency-thickness 2 MHz.mm, for an EMAT wavelength of 22 mm), Figure 1 shows that one would expect to obtain a strongly dispersive SH_1 mode, with SH_0 possibly also generated if the spatial and temporal bandwidth is large enough [8] [11]. Figure 5 shows sonograms of the signal produced using the miniaturised generation and detection EMATs on 10 mm thick steel. Generation at 200 kHz used a different number of cycles, for a relatively broadband pulse when using 1 cycle (Figure 5(a), for generation using Design 1 and detection using Design 3, denoted as 1-3 throughout the rest of this paper), 3 cycles (Figure 5(b)), and a more narrowband pulse when using 6 cycles (Figure 5(c), same EMATs). For comparison, Figure 5 (d) and (e) show wavemodes generated by a commercial transducer pair which has 20 mm wavelength. 3 cycle excitation was used, at two frequencies: 200 kHz gives the same frequency-thickness as used for the miniature EMATs, while

220 kHz gives the optimal generation frequency for this wavelength. 20 mm wavelength was chosen as the closest option to 22 mm available commercially. Finally, the signal from a more broadband combination of miniaturised transducer designs (using design 3 as both generator and detector) is shown in Figure 5(f), with excitation using 3 cycles.

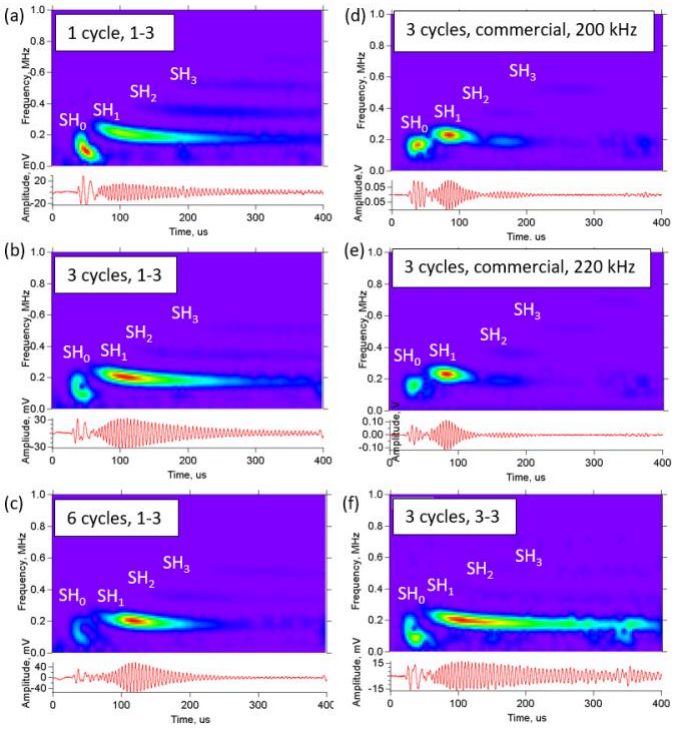

Figure 5: Frequency-time representation (sonogram) of the generated signal on 10 mm steel using miniaturised EMAT pairs (λ=22 mm) excited at 200 kHz, or a matched commercial transducer pair (λ=20 mm) excited at 200 kHz or 220 kHz; 16 averages used in all cases. The numbers correspond to the generation and detection design. (a) Design 1-3, short pulse (1 cycle) excitation, (b) design 1-3, 3 cycles excitation, (c) design 1-3, 6 cycles excitation, (d) commercial transducer pair with λ=20mm 3 cycles at 200kHz and at (e) 220kHz; (f) design 3-3, 3 cycles excitation.

The miniaturised transducer pairs are shown to have a broader bandwidth than the commercial EMATs by the extent of the signals in the sonograms, as expected from the design. For excitation using a single cycle (most broadband), more energy is distributed into the higher SH modes (SH_2, SH_3) as well as into the SH_0 mode, relative to SH_1, as seen from comparing Figures 5 a, b and c. Both SH_0 and SH_1 modes are generated in all cases, including with the narrowband commercial pair. The coincidental generation of the SH_0 mode can be used to advantage: the SH_0 mode is non-dispersive and can be used as a reference signal to compare velocity changes of higher order modes to, in order to remove any effect due to variation in transducer separation. In addition, generation of higher order modes can be used when performing thickness gauging, for investigation of the cut-off of these modes as the thickness is reduced [6] [15] or discontinuities encountered [23].

Three cycles of excitation was chosen for further study. The choice of the optimal number of cycles depends on the particular application. The optimisation takes into account the desired distance between the generator and detector, arrival times of the modes (as defined by their group velocities from dispersion curves), and the desired SNR. These parameters are interlinked. With more cycles of excitation, there is more overlap between the modes which can cause issues with separating the modes for analysis. The overlap can be reduced by placing transducers further apart, but this reduces the amplitude and thus SNR of the dispersive SH_1 mode. However, with more cycles of excitation, the SH_1 mode is generated more efficiently (Figure 5). This gives a lot of freedom for design and the choice ultimately depends on the geometry of the sample for testing by the transducer pair.

B. Directivity

Directivity of the miniature EMATs was tested at 200 kHz, with the results for the SH_0 and SH_1 wavemodes shown in Figure 6 for designs 1, 2 and 3 used as generators, with design 4 used as a detector. Each design shows a main lobe, with some side lobes at higher angles. Note that there is signal generated in the opposite direction as well; this is not shown on the graphs. As expected, design 1 has higher directivity (narrower main lobe) compared to design 2, which has a narrower wavefront, and the difference becomes more pronounced when comparing with design 3, which has only one row of magnets. The directivity of generation of the tested EMATs measured in this way is similar to their directivity behaviour as detectors.

The directivity of design 1 means that it is suitable for most applications, including where waves are required to travel larger distances. Design 2 is also suitable as a generator for applications where signals do not need to cover a long distance before being detected. Design 3 has poor directivity but, as shown by the sonograms, still produces reasonable signal when used in a pitch-catch arrangement at 300 mm separation (Figure 5(f)). It is most promising as a detector, as it is sensitive to a wide range of directions of incident waves.

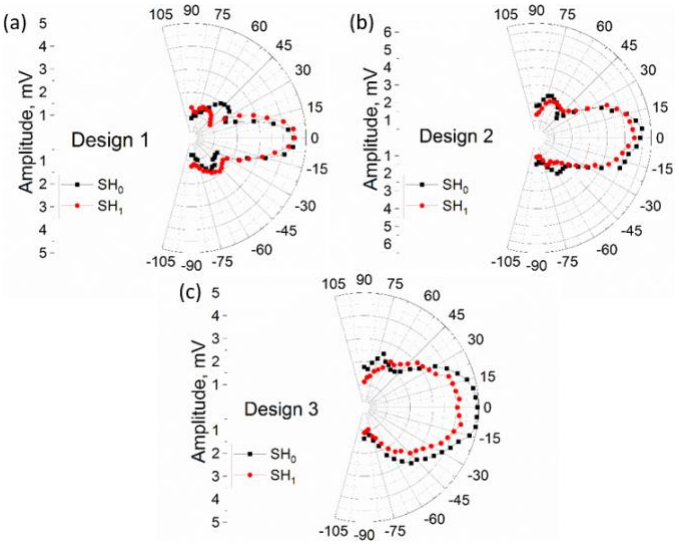

Figure 6: Directivity of EMATs with designs 1, 2 and 3 operated as generators, and design 4 used as a detector due to its small footprint (width of active area 6 mm). SH_0 (black squares) and SH_1 (red circles) were excited with a 3 cycle pulse at 200 kHz.

C. SNR and magnetic drag comparison

Magnetic drag was measured at several different places on

the sample for each EMAT design, with the results averaged, in order to reduce issues due to material variations dependent on the exact position each EMAT was initially placed. Typical forces measured using EMAT design 2 are shown in Figure 7(a), for different pushing times. The mean drag force for each EMAT design is plotted in Figure 7(b), with error bars calculated using standard deviation. The commercial EMATs were tested using a larger roller (with radius 3 times that of the smaller roller), with results from these measurements labelled as A. If the small roller had been used, the friction force would have increased by a factor of 3, as can be seen from Equation (3). The calculated force for if the small roller was used instead is labelled as B; note that this could not be tested experimentally as it was above the maximum drag force for the robot. The maximum values for the drag force in normal operation, and for short, peak pull operation, are shown by the dashed lines. All miniaturised EMATs are well below the normal pull drag force, while the commercial EMAT is below this only if the large roller is used, and for using a single EMAT only, limiting the potential scope of measurements. EMATs are used in pairs for defect measurements, and hence the drag force when pulling two EMATs must be considered when confirming whether the robot is capable of performing the scanning. Table 1 gives the drag force for pairs of EMATs, calculated by adding the force values for the corresponding EMAT combinations.

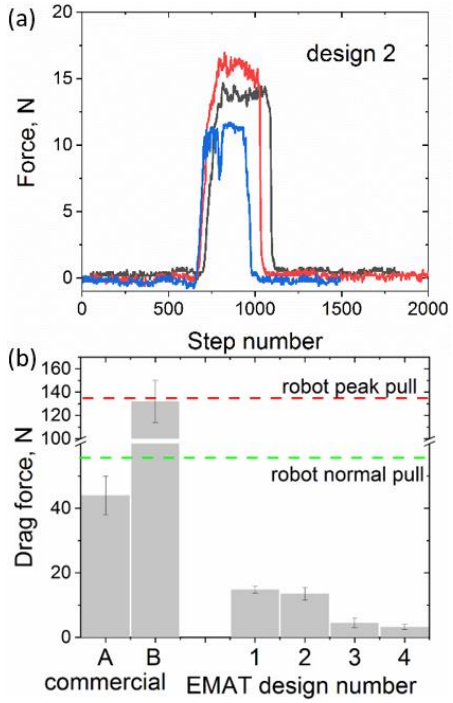

Figure 7: Drag force measurement for single EMATs: (a) force profile when pushing, over three different positions on the sample, for EMAT design 2; (b) drag forces for each EMAT design. For the commercial EMAT A corresponds to the large roller with radius $r_{large}=3r_{small}$, while B shows the calculated force for the small roller with radius r_{small}.

SNR has been tested for different EMAT pair combinations to ensure that miniaturisation does not reduce SNR to a level which does not permit experiments. The EMAT pairings were chosen to ensure significant drag reduction compared to the commercial transducers, in particular for scenarios using two detectors, as envisaged in figure 3(b). Figure 8 shows the comparison of signals obtained using a commercial EMAT pair with 20 mm wavelength and from miniaturised EMAT pairs with 22 mm wavelength. All measurements were conducted using 3 cycle excitation at 200 kHz, for 16 averages, with 300 mm distance between generator and detector centres. All measurements were done at the same position on a 10 mm thick steel plate for 0.1 mm lift-off between EMAT and sample. The differences in the shape of the observed signals between commercial and miniaturised EMATs are because the wavelengths of the transducers are slightly different, and because the commercial EMATs are narrowband due to the PPM design used, while the miniature EMATs are inherently broadband. Despite these minor differences, the measurements allow for a meaningful comparison of SNR.

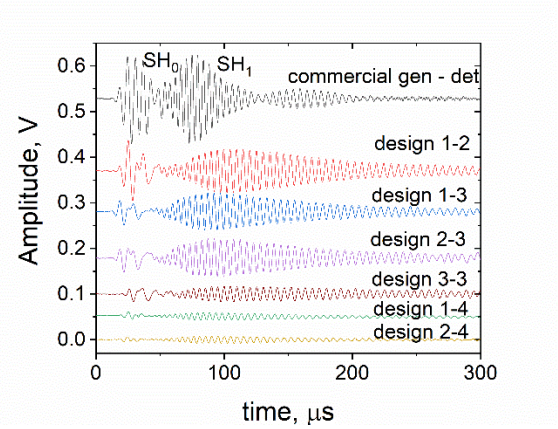

Figure 8: Signals produced at 200 kHz, 3 cycles, using commercial EMATs with 20 mm wavelength, and miniaturised EMAT pairs in most viable combinations.

TABLE I
SIGNAL TO NOISE RATIO AND MAGNETIC DRAG

EMAT pair (first is generator design number, second is detector)		SNR amplitude ratio		SNR (dB)		Experimental drag force calculated for pair (kg)
		SH_0	SH_1	SH_0	SH_1	
Sonemat Ltd. SHG/D2031s	200 kHz	62	62	36	36	8.8 ±1.2 (26.4 ± 3.6)
Sonemat Ltd. SHG/D2031s	220 kHz	53	69	35	37	
1-2		43	31	33	30	2.9 ± 0.3
1-3		17	26	25	28	2 ± 0.3
2-3		17	26	25	28	1.8 ± 0.4
3-3		10	11	20	21	0.9 ± 0.3
1-4		6	6	15	15	1.8 ± 0.2
2-4		4	5	12	14	1.7 ± 0.1

Signal to noise ratio and drag force comparison between a commercial pair of transducers (excited at 200 kHz or 220 kHz) and combinations of miniaturised EMAT pairs excited at 200 kHz (3 cycles) for SH_0 and SH_1 wavemodes. The bracketed value is the estimate of the force expected for the commercial EMATs for the same experimental conditions as measured for the miniaturised EMATs.

As expected, the miniaturised EMATs have a reduced SNR compared to commercial options, but it is sufficient for experiments for all designs with the two primary SH wavemodes clearly observable above the noise level on all traces. The SNR values of the tested transducers for both SH_0 and SH_1 modes at 200 kHz excitation, as well as with 220 kHz excitation for the commercial pair (ensuring comparison is done at the optimal frequency for all EMATs) are summarised in Table 1 together with the corresponding drag forces. SNR can

be expressed as a ratio of signal amplitude to noise amplitude, a ratio of power (square) of these amplitudes or on a logarithmic scale (dB). The ratio of signal and noise amplitudes is given here, alongside the corresponding number in dB. The noise amplitude was measured over the first 15 ms of signal in Figure 8, before the arrival of the SH_0 mode.

Experiments using designs 1-2, 1-3 and 2-3 (generator-detector) have similar performance and show very similar wave shapes in figure 8. This would change if different separation was used, as design 2 has lower directivity than design 1, and therefore the energy of the wave would dissipate faster with increasing separation as the wave spread out more. Design 1-2 is slightly more efficient, in particular when generating the SH_0 mode. This is expected as this pair uses the largest EMATs out of these three set-ups, and higher sensitivity to a non-dispersive SH_0 is expected because the design 1-2 combination is more narrowband. The difference in shapes of the wavemodes when using the commercial EMAT pair is due to the high periodicity of the commercial design, which leads to more cycles appearing in each signal. The unavoidable wavelength difference between the commercial and the miniaturised EMATs also has an effect, as this puts them in slightly different positions on the dispersion curve. This results in the SH_1 mode generated by the commercial EMAT having a lower dispersion, and hence appearing to be more compact with a higher amplitude.

The maximum pulling weight of the robot used is 13.5 kg, considering all contributing factors such as payload weight and magnetic drag, and this value cannot be sustained for long periods of time. The commercial EMAT pair can be pulled by this robot when using rolling friction and the large rollers, but only for short-term operation, as the force experienced by the robot is above its normal operational level. In contrast, all combinations of miniaturised EMATs have drag forces well within the operational range of the robot. It is worth noting that some EMAT combinations offer a more optimal choice: for example, pairs 2-3 and 1-4 have similar magnetic drag, but SNR is much higher for the first of these, and therefore it would be a more optimal choice for inspection.

Further increasing the lift-off of the commercial transducers can lead to reducing the pulling weight sufficiently that they can be used. By increasing the lift-off to 2 mm, the drag force was reduced to 1.8 kg per EMAT, giving a total of 3.6 kg for the pair. However, this leads to a significant reduction in SNR, bringing it to the same level as that of miniaturised pair 1-3, which has a drag force of 2 kg (Table 1). The miniaturisation process therefore offers better SNR with useable drag forces for robotic crawler implementation than using commercial EMATs at a higher lift-off, and offers other benefits when considering the generation of multiple wavemodes.

D. Defect scanning

It is important to test the suitability of the miniature EMATs for defect detection. Pairs 1-2, 1-3 and 2-3 have sufficient SNR and acceptable magnetic drag for robotic scanning. EMAT design 1 was chosen as generator to demonstrate that these designs could be effective for defect detection, based on its better directivity. Design 3 was chosen as detector based on its low magnetic drag, to ensure that scanning was as easy as possible. 3 cycles excitation was used as it gives a good balance between bandwidth and SNR, and pulse duration (and therefore temporal resolution) when analysing the data.

To demonstrate defect detection a simple analysis was chosen, looking at the amplitudes of the SH_1 mode. A bandpass filter was used to reduce noise and unwanted modes. SH_1 amplitudes are shown in figure 9 for a line scan over an area without defects, and over another area containing a defect (5 mm deep, 40 mm diameter flat bottomed hole). The plate inspected was 1500 mm in length but only 300 mm in width, and reflections from the side edges affected the measurements. The average amplitude of SH_1 mode away from the defect is shown by dashed lines (this represents background). The SH_1 mode amplitude is reduced when the defect is between the EMATs. The mechanism behind the amplitude reduction of the transmitted waves is complex; mode conversions and interference are likely to be present and may be responsible for the profile observed in the scan, alongside effects due to the finite size of the EMATs.

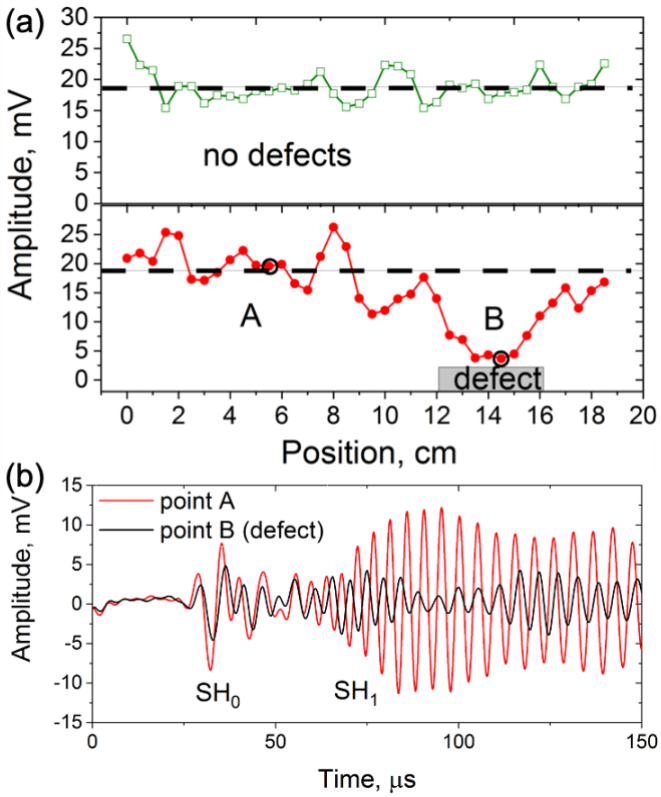

Figure 9: Sample scanning. (a) SH1 amplitude for a scan over a clear area of the plate (green open circles) and over the area with 40mm diameter, 5mm deep defect (red filled circles). The black dashed line illustrates the baseline signal level. Two points on the scan over the defected area - when the transducers are away from the defect and when the defect is directly between the transducers – are plotted in (b).

Figure 9 (b) shows example pitch-catch signals acquired with the defect exactly between the EMATs, and when the EMATs are away from the defect area for both scans. This more detailed view shows that both the SH_1 amplitude and arrival time are affected, while the SH_0 wave remains mostly unchanged, as expected for a non-dispersive mode.

Even when simply analysing just the amplitudes of the SH_1 mode, the non-defect areas can be separated from the regions with flat bottomed holes by measuring a reduction in

transmitted SH_1 signal when defects are present. The shape of the defect and the gradient of wall thinning will affect mode conversions, and this will have a complex influence on the SH_0 and SH_1 amplitudes, so more complex processing is required. A combination of changes in amplitude and arrival times of the modes is showing the potential for use in commercial applications [15]. The level of detail in these scans has many benefits compared to measurements at single points, and the miniaturised EMATs described here offer the ability to easily scan samples.

V. Conclusions

Miniature guided SH wave EMATs have been developed for the industrially relevant case of measuring wall thinning in 10 mm thick ferritic steel plate. The SNR of the miniaturized EMATs is moderately reduced compared to the traditional design commercial PPM-EMATs, but is within acceptable limits for operation. EMAT miniaturisation makes a significant difference in drag forces and enables the use of long wavelength EMATs on crawler robots. An artificial defect (flat bottomed hole) representing 50% wall thinning with lateral dimensions just under 2 wavelengths was successfully detected using a small EMAT pair.

The miniaturisation principle can be applied to produce miniaturised EMATs operating at other wavelengths. The optimal balance between size, drag force, directivity, bandwidth and SNR should be chosen for a particular application. The more extreme cases of miniaturisation have been presented here. Intermediate sizes are expected to have an intermediate performance in terms of the mentioned parameters (drag force, directivity, bandwidth, SNR). The described design approach is promising for implementation onto a robotic inspection system, paving the way for non-contact guided wave robotic inspection of steel structures, using small crawler robots.

References

[1] Eddyfi, [Online]. Available: https://www.eddyfi.com/en/product/scorpion-2. [Accessed 04 2020].

[2] G. Dobbie and G. Pierce, IEEE SENSORS JOURNAL, vol. 11, no. 10, pp. 2458-2468, 2011.

[3] J. Rose, Ultrasonic waves in solid media, Cambridge University Press , 2014.

[4] C. F. Vasile and R. B. Thompson, "Excitation of horizontally polarized shear elastic waves by electromagnetic transducers with periodic permanent magnets c. F. Vasile and R. B. Thompson," Journal of Applied Physics, vol. 50, p. 2583, 1979.

[5] M. Hirao and H. Ogi, "An SH-wave EMAT technique for gas pipeline inspection," NDT & E International, vol. 32, no. 3, pp. 127-132, 1999.

[6] A. C. Kubrusly, M. A. Freitas, J. P. von der Weid and S. M. Dixon, "Interaction of SH guided waves with wall thinning," NDT&E International, vol. 101, pp. 94-103, 2019.

[7] P. Khalili and P. Cawley, "The choice of ultrasonic inspection method for the detection of corrosion at inaccessible locations", vol 99, pp 80-92, 2018," NDT and E International, vol. 99, pp. 80-92, 2018.

[8] S. M. Dixon, P. A. Petcher, Y. Fan, D. Maisey and P. Nickolds, "Ultrasonic metal sheet thickness measurement without prior wave speed calibration," J Phys D: Appl. Phys.,, vol. 46, p. 445502, 2013.

[9] P. A. Petcher, S. E. Burrows and S. M. Dixon, "Shear horizontal (SH) ultrasound wave propagation around smooth corners," Ultrasonics, vol. 54, pp. 997-1004, 2014.

[10] P. A. Petcher and S. M. Dixon, "Weld defect detection using PPM EMAT generated shear horizontal ultrasound," NDT & E International, vol. 74, pp. 58-65, 2015.

[11] M. Clough, M. Fleming and S. M. Dixon, "Circumferential guided wave EMAT system for pipeline screening using shear horizontal ultrasound," NDT & E International, vol. 86, pp. 20-27, 2017.

[12] M. Hirao and H. Ogi, EMATs for science and industry. Noncontacting ultrasonic measurements, Kluwer Academic Publishers, 2003.

[13] R. Murayama, S. Makiyama, M. Kodama and Y. Taniguchi, "Development of an ultrasonic inspection robot using an electromagnetic acoustic transducer for a Lamb wave and an SH-plate wave," Ultrasonics, vol. 42, pp. 825-829, 2004.

[14] O. Trushkevych and R. S. Edwards, "Characterisation of small defects using miniaturised EMAT system," NDT&E International, vol. 107, p. 102140, 2019.

[15] P. A. Petcher and S. M. Dixon, "Mode mixing in shear horizontal ultrasonic guided waves," Nondestr Testing & Eval, vol. 32, no. 2, pp. 113-132, 2017.

[16] R. Ribichini, F. Cegla, P. B. Nagy and P. Cawley, "Study and comparison of different EMAT configurations for SH wave inspection," IEEE Transactions on Ultrasonics, Ferroelectrics and Frequency Control, vol. 58, no. 12, pp. 2571- 2581, 2011.

[17] O. Trushkevych, S. M. Dixon, M. Tabatabaeipour, G. Dobbie, M. D. Potter, C. MacLeod, A. Gachagan, S. G. Pierce and O. Trushkevych, "Towards Guided Wave Robotic NDT Inspection: EMAT Size Matters"," IEEE 2019 IUS Proceedings, p. under review, 2019.

[18] S. Choi, H. Cho and C. J. Lissenden, "Selection of Shear Horizontal Wave Transducers for Robotic Nondestructive Inspection in Harsh Environments," Sensors, p. 17(1):5, 2016.

[19] X. Song and G. Qiu, "Optimization of a Focusable and Rotatable Shear-Wave Periodic Permanent Magnet Electromagnetic Acoustic Transducers for Plates Inspection," Sensors, vol. 17, p. 2722, 2017.

[20] H. Sun, S. Huang, Q. Wang, S. Wang and W. Zhao, "Improvement of unidirectional focusing periodic permanent magnet shear-horizontal wave electromagnetic acoustic transducer by oblique bias magnetic field," Sensors and Actuators A: Physical, vol. 290, pp. 36-47, 2019.

[21] [Online]. Available: http://inuktun.com/en/products/onsite-standard-products/micromag-miniature-magnetic-crawler/. [Accessed 12 2019].

[22] J. He, S. M. Dixon, S. Hill and K. Xu, "A New Electromagnetic Acoustic Transducer Design for Generating and Receiving S0 Lamb Waves in Ferromagnetic Steel Plate," Sensors, vol. 17, p. 1023, 2017.

[23] A. C. Kubrusly, J. P. von der Weid and S. Dixon, "Experimental and numerical investigation of the interaction of the first four SH guided wave modes with symmetric and non-symmetric discontinuities in plates," NDT & E International, vol. 108, p. 102175, 2019.

[24] H. Nurmalia, N. Nakamura, H. Ogi, M. Hirao and K. Nakahata, "Mode conversion behavior of SH guided wave in a tapered plate," NDT&E International, vol. 45, p. 156–161, 2012.

[25] O. Trushkevych and R. S. Edwards, "Differential coil EMAT for simultaneous detection of in-plane and out-of-plane components of surface acoustic waves," IEEE Sensors Journal, vol. Early Access, pp. 1-7, 2020.

[26] S. L. Huang, H. Y. Sun, Q. Wang, S. Wang and W. Zhao, "Unidirectional focusing of horizontally polarized shear elastic waves electromagnetic acoustic transducers for plate inspection," J. Appl. Phys., vol. 125, p. 164504, 2019.

[27] M. Tabatabaeipour and et al, " Bayesian Robotic Mapping using Ultrasonic Guided Waves", submitted to IEEE Transactions on Automation Science and Engineering, 2020.

[28] "https://www.singletact.com," [Online]. [Accessed 20 05 2020].